Buoyancy Driven Heat Transfer of Nanofluids in a Tilted Enclosure

Kamil Kahveci[1]
Department of Mechanical Engineering,
Trakya University,
22180 Edirne, Turkey
e-mail: kamilk@trakya.edu.tr

Buoyancy driven heat transfer of water-based nanofluids in a differentially heated, tilted enclosure is investigated in this study. The governing equations (obtained with the Boussinesq approximation) are solved using the polynomial differential quadrature method for an inclination angle ranging from 0 deg to 90 deg, two different ratios of the nanolayer thickness to the original particle radius (0.02 and 0.1), a solid volume fraction ranging from 0% to 20%, and a Rayleigh number varying from 10^4 to 10^6. Five types of nanoparticles, Cu, Ag, CuO, Al_2O_3, and TiO_2 are taken into consideration. The results show that the average heat transfer rate from highest to lowest is for Ag, Cu, CuO, Al_2O_3, and TiO_2. The results also show that for the particle radius generally used in practice ($\beta=0.1$ or $\beta=0.02$), the average heat transfer rate increases to 44% for $Ra=10^4$, to 53% for $Ra=10^5$, and to 54% for $Ra=10^6$ if the special case of $\theta=90$ deg, which also produces the minimum heat transfer rates, is not taken into consideration. As for $\theta=90$ deg, the heat transfer enhancement reaches 21% for $Ra=10^4$, 44% for $Ra=10^5$, and 138% for $Ra=10^6$. The average heat transfer rate shows an increasing trend with an increasing inclination angle, and a peak value is detected. Beyond the peak point, the foregoing trend reverses and the average heat transfer rate decreases with a further increase in the inclination angle. Maximum heat transfer takes place at $\theta=45$ deg for $Ra=10^4$ and at $\theta=30$ deg for $Ra=10^5$ and 10^6. [DOI: 10.1115/1.4000744]

Keywords: natural convection, nanofluid, enclosure, PDQ, vorticity, stream function

1 Introduction

As is well known, conventional heat transfer fluids such as water, ethylene glycol, and oil have low thermal conductivities. This is the main drawback in enhancing the performance and the compactness of many engineering devices. Therefore, there is a strong need for advanced heat transfer fluids with substantially higher thermal conductivities. The way to eliminate this need is to use solid particles within a base fluid. Because of technological difficulties, micron-sized particles have been used in the past, but sedimentation and clogging were persistent problems in fluids with micron-sized particles. The introduction of nanofluids has eliminated these drawbacks. The term nanofluid is used to describe a solid and liquid mixture that consists of a base liquid and nanoparticles sized less than 100 nm. Ceramic particles (Al_2O_3, CuO, TiO_2, SiC, and SiO_2), pure metallic particles (Cu, Ag, Au, and Fe), and carbon nanotubes are all used as nanoparticles. The presence of the nanoparticles causes an anomalous increase in the effective thermal conductivity of the fluid. Eastman et al. [1] found that the effective thermal conductivity of ethylene glycol increases up to 40% for a nanofluid consisting of ethylene glycol containing approximately 0.3 vol % Cu nanoparticles of mean diameter less than 10 nm. Choi et al. [2] produced nanotube-in-oil suspensions and measured their effective thermal conductivity. The measured thermal conductivity found to be anomalously greater than theoretical predictions and nonlinear with nanotube loadings. Xuan and Li [3] made a theoretical study of the thermal conductivity of nanofluids. The hot-wire apparatus was used to measure the thermal conductivity of nanofluids with suspended copper nanophase powders. They found that for the water-copper nanoparticle suspension, the ratio of the thermal conductivity of the nanofluid to that of the base liquid varies from 1.24 to 1.78 if the volume fraction of the ultrafine particles increases from 2.5% to 7.5%. Das et al. [4] investigated the increase in thermal conductivity with temperature for nanofluids with water as base fluid and particles of Al_2O_3 or CuO as suspension material. The results indicate an increase in enhancement characteristics with temperature, which makes the nanofluids even more attractive for applications with high energy density than usual room temperature measurements reported earlier. Keblinski et al. [5] investigated four possible mechanisms for this anomalous increase: Brownian motion of the nanoparticles, molecular level layering of the liquid at the liquid-particle interface, the nature of heat transfer in the nanoparticles, and nanoparticle clustering. Keblinski et al. [5] also showed that the Brownian motion is a negligible contributor, and that liquid layering around the nanoparticles could cause rapid conduction.

Thermal conductivity is the most important parameter for the heat transfer enhancement potential of nanofluids. It is known that the thermal conductivity of a nanofluid is a function of the thermal conductivity of both the base fluid and the nanoparticle, the volume fraction, the surface area, the shape of the nanoparticles, and the distribution of the dispersed particles. However, there are no theoretical formulas currently available in the literature for predicting the thermal conductivity of the nanofluids. Some proposed models do exist for solid-liquid mixtures with micrometer-sized particles. In these models, the thermal conductivity of the suspensions depends only on the volume fraction and shape of the suspended solid particles, but not on the size and distribution of the particles. In the absence of a suitable theory for nanofluids, models for the solid-liquid suspensions with relatively large particles may be extended to estimate the thermal conductivity of the nanofluids.

The most popular thermal conductivity model for this type of solid-liquid mixture is the Maxwell model [6]; this is the model on which most later-proposed models for nanofluids are based. In this model, the thermal conductivity is defined as follows:

[1]Present address: Muhendislik Mimarlik Fakultesi, Trakya Universitesi, 22030 Edirne, Turkey.

Contributed by the Heat Transfer Division of ASME for publication in the JOURNAL OF HEAT TRANSFER. Manuscript received March 25, 2009; final manuscript received October 9, 2009; published online March 24, 2010. Assoc. Editor: Yutaka Asako.

$$k_{\text{eff}}/k_f = \frac{k_s + 2k_f + 2(k_s - k_f)\phi}{k_s + 2k_f - (k_s - k_f)\phi} \quad (1)$$

where k_s is the thermal conductivity of the particle, k_f is the thermal conductivity of the base fluid, and ϕ is the solid particle volume fraction. In this traditional model, the effective thermal conductivity of the suspensions depends on the thermal conductivity of the spherical particle, the base liquid, and the volume fraction of the solid particles.

The thermal conductivity of nanofluids with nonspherical particles depends not only on the volume fraction of the particles, but also on the shape of the particles. Hamilton and Crosser [7] proposed a model for the effective thermal conductivity of two-component mixtures with nonspherical particles. In this model, given below, thermal conductivity is a function of the conductivity of both the particle and the base fluid, as well as the shape of the particles

$$k_{\text{eff}}/k_f = \frac{k_s + (n-1)k_f + (n-1)(k_s - k_f)\phi}{k_s + (n-1)k_f - (k_s - k_f)\phi} \quad (2)$$

Here, n is the empirical shape factor: $n=3/\Psi$, where Ψ is the sphericity (i.e., the ratio of the surface area of a sphere with a volume equal to that of the particle to the surface area of the particle). The shape factor n can vary from 0.5 to 6.0 (a sphere $=3$, a cylinder$=6$).

An alternative expression for calculating the effective thermal conductivity of solid-liquid mixtures has been proposed by Yu and Choi [8]. They claimed that a structural model of nanofluids might consist of a bulk liquid, solid nanoparticles, and solid-like nanolayers. The solid-like nanolayers act as a thermal bridge between a solid nanoparticle and a bulk liquid. With the assumption of $k_{\text{layer}}=k_p$, the model for spherical nanoparticles is as follows:

$$k_{\text{eff}}/k_f = \frac{k_s + 2k_f + 2(k_s - k_f)(1+\beta)^3\phi}{k_s + 2k_f - (k_s - k_f)(1+\beta)^3\phi} \quad (3)$$

where β is the ratio of the nanolayer thickness to the original particle radius. Yu and Choi [8] compared their model results for $\beta=0.1$ with existing experimental results in literature and obtained a reasonably good agreement. The prediction is effective, most particularly when the nanoparticles have a diameter of less than 10 nm. This model has been used in the present study to define the effective thermal conductivity of the nanofluids.

The viscosity of the nanofluid is generally estimated using existing relations for a two-phased mixture. The following equation given by Brinkman [9] was used as the relation for the effective viscosity in this investigation:

$$\mu_{\text{eff}} = \mu_f/(1-\phi)^{2.5} \quad (4)$$

Xuan et al. [10] experimentally measured the effective viscosity of the transformer oil-water nanofluid and of the water-copper nanofluid in the temperature range of 20–50 °C. Their experimental results showed reasonably good agreement with the theory by Brinkman [9].

There is a relatively limited number of studies on convective heat transfer of nanofluids. In one of these studies, Xuan and Li [11] found that nanofluids with oxide particles generally cause a moderate increase in heat transfer while a significant enhancement is obtained for nanofluids with metallic particles. This is because of the fact that a high enhancement rate for metallic nanofluids requires only a small solid volume fraction that does not affect the viscosity significantly. In another study, Eastman et al. [12] found that with less than 1% volume fraction of CuO, the convection heat transfer rate increased by more than 15% in water. Wen and Ding [13] studied laminar heat transfer in the entrance region of a tube flow with an alumina-water nanofluid and found that with a 1.6% solid volume fraction, the local heat transfer coefficient at the entrance region takes on a value that is 41% higher than that at the base fluid with the same flow rate. Wen and Ding [13] also observed that the enhancement is particularly significant in the entrance region and decreases with axial distance. Maiga et al. [14] numerically studied laminar and turbulent flows of nanofluids in a uniformly heated tube for using approximated correlations for experimental data. They found that the heat transfer enhancement due to the nanoparticles becomes more important for the turbulent flow regime with an increase in the Reynolds number. Maiga et al. [15] also studied forced convection flows of nanofluids in a uniformly heated tube and a system of parallel, coaxial, and heated disks. They found that both the Reynolds number and the gap between disks have an insignificant effect on the heat transfer enhancement. Akbarinia and Behzadmehr [16] studied laminar, mixed convection of an Al_2O_3-based nanofluid in a horizontal curved tube. They found that for a given nanoparticle concentration, increasing the buoyancy forces caused a reduction in the skin friction. Mirmasoumi and Behzadmehr [17] studied laminar mixed convection of an Al_2O_3-based nanofluid. The results showed that increasing the nanoparticle volume fraction increases the secondary flow strength. Mirmasoumi and Behzadmehr [17] also observed that the skin friction coefficient in the fully developed region does not notably change with an increasing solid volume fraction, except for at the entrance region. In another study, Izadi et al. [18] made a numerical investigation on developing laminar forced convection of a nanofluid consisting of Al_2O_3 and water in an annulus and observed that the dimensionless axial velocity profile does not significantly change with the nanoparticle volume fraction. However, the temperature profiles are affected by the nanoparticle concentration. Khanafer et al. [19] studied natural convection of copper-based nanofluids in a differentially heated square cavity. Their results show that the presence of nanoparticles enhances heat transfer by about 25% for Gr $=10^4$ and Gr$=10^5$ at a volume fraction of $\varphi=0.2$. In another study similar to that done by Khanafer et al. [19], Santra et al. [20] observed that the heat transfer decreases with an increase in φ for a particular Ra, while it increases with Ra for a particular φ. Buoyancy driven heat transfer of water-based Al_2O_3 nanofluids in a rectangular cavity was studied theoretically by Hwang et al. [21]. They found that water-based Al_2O_3 nanofluids is more stable than base fluid in a rectangular cavity heated from below as the volume fraction of nanoparticles increases, the size of nanoparticles decreases, or the average temperature of nanofluids increases. They also found that the ratio of the heat transfer coefficient of nanofluids to that of the base fluid is decreased as the size of nanoparticles increases, or the average temperature of nanofluids is decreased. The heat transfer enhancement of a copper-based nanofluid in a two-dimensional enclosure was investigated by Jou and Tzeng [22]. It was shown that the average Nusselt number at the hot wall is increased as the aspect ratio decreased. Oztop and Abu-Nada [23] studied buoyancy driven heat transfer and fluid flow in a partially heated enclosure using nanofluids. They observed that the heat transfer enhancement is more pronounced at low aspect ratios than at high aspect ratios of the enclosure. Aminossadati and Ghasemi [24] investigated natural convection cooling of a heat source embedded on the bottom wall of an enclosure filled with nanofluids and found that the type of nanoparticles and the length and location of the heat source affect the heat source maximum temperature significantly. Heat transfer augmentation in a two-sided lid-driven differentially heated square cavity utilizing nanofluids was studied numerically by Tiwari and Das [25]. They observed that when both the vertical walls move upwards in the same direction, the heat transfer is reduced. They also found that when the vertical walls move in opposite directions, the heat transfer is considerably enhanced for forced convection dominated regime regardless of which side moves upwards. Koo and Kleinstreuer [26] investigated the microheat sink and found that a high-Prandtl number base fluid and a high aspect ratio channel give better heat transfer performance.

As also seen from the above literature, there is a relatively limited number of studies on convective heat transfer of nanofluids in an enclosure, while convective heat transfer of conven-

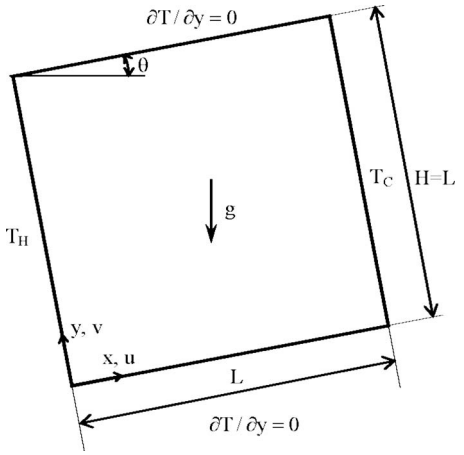

Fig. 1 Geometry and coordinate system

tional heat transfer fluids (see Refs. [27–40]) has been studied extensively. The present study therefore aims to investigate the effects of several pertinent parameters on the flow and heat transfer characteristics of water-based nanofluids in a tilted enclosure using the polynomial differential quadrature (PDQ) method.

2 Analysis

The basic flow configuration used in the analysis is shown in Fig. 1. The tilted square enclosure of height H and width L is bounded by two isothermal walls at temperatures T_H and T_C, and two adiabatic walls. The flow is assumed to be Newtonian, two-dimensional, steady, and incompressible. Despite the fact that a nanofluid is a two phase mixture, since the solid particles are of a very small size, they are easily fluidized and therefore can be considered to behave as a fluid. Therefore, it might be reasonable to treat a nanofluid as a single phase flow. The single phase approach assumes that the fluid phase and particles are in thermal equilibrium and move with the same velocity. This approach, which is simpler and requires less computational effort, is used in this study.

In order to nondimensionalize the governing equations, the following dimensionless variables are used:

$$x = \frac{x^*}{L}, \quad y = \frac{y^*}{L}, \quad u = \frac{u^*}{\alpha_f/L}, \quad v = \frac{v^*}{\alpha_f/L}, \quad p = \frac{L^2}{\rho_{fo}\alpha_f^2}p^*$$
$$T = \frac{T^* - T_C}{T_H - T_C} \tag{5}$$

where u^* and v^* are the dimensional velocity components, p^* is the dimensional pressure, T^* is the dimensional temperature, ρ_f is the fluid density, and α is the thermal diffusivity of the fluid. As shown in detail by Gill [41], the scaling in Eqs. (6) and (7) is based on the balance between the convective and conductive terms in the energy equation, and on the balance between the buoyancy and diffusion terms in the momentum equation.

The buoyancy effects are incorporated in the formulation by invoking the Boussinesq approximation. The viscous dissipation terms and the thermal radiation are assumed to be negligible. With the foregoing assumptions, the dimensionless governing equations can be given as follows in the vorticity-stream function formulation:

$$\frac{\partial^2\psi}{\partial x^2} + \frac{\partial^2\psi}{\partial y^2} = -\omega \tag{6}$$

$$u\frac{\partial\omega}{\partial x} + v\frac{\partial\omega}{\partial y} = \frac{\gamma_{\text{eff}}}{\gamma_f}\text{Pr}\left(\frac{\partial^2\omega}{\partial x^2} + \frac{\partial^2\omega}{\partial y^2}\right) + \frac{(\rho\beta_T)_{\text{eff}}}{\rho_{\text{eff}}\beta_{T,f}}\text{Ra}\ \text{Pr}\left[\cos\theta\frac{\partial T}{\partial x} - \sin\theta\frac{\partial T}{\partial y}\right] \tag{7}$$

$$u\frac{\partial T}{\partial x} + v\frac{\partial T}{\partial y} = \frac{\alpha_{\text{eff}}}{\alpha_f}\left[\frac{\partial^2 T}{\partial x^2} + \frac{\partial^2 T}{\partial y^2}\right] \tag{8}$$

Here the Prandtl and Rayleigh numbers are defined as

$$\text{Pr} = \frac{\gamma_f}{\alpha_f}, \quad \text{Ra} = \frac{g\beta_{T,f}L^3\Delta T^*}{\gamma_f\alpha_f} \tag{9}$$

where g is the gravitational acceleration, β_T is the coefficient of thermal expansion, and γ is the kinematic viscosity. ΔT^* is the temperature difference between the isothermal walls of the enclosure. The effective properties present in the governing equations can be expressed by the following relations:

$$(\rho C_p)_{\text{eff}} = (1-\phi)(\rho C_p)_f + \phi(\rho C_p)_s \tag{10}$$

$$(\rho\beta_T)_{\text{eff}} = (1-\phi)(\rho\beta_T)_f + \phi(\rho\beta_T)_s \tag{11}$$

where

$$\rho_{\text{eff}} = (1-\phi)\rho_f + \phi\rho_s \tag{12}$$

The dimensionless stream function and vorticity in Eqs. (6) and (7) are defined as follows:

$$u = \frac{\partial\psi}{\partial y}, \quad v = -\frac{\partial\psi}{\partial x}, \quad \omega = \frac{\partial v}{\partial x} - \frac{\partial u}{\partial y} \tag{13}$$

The appropriate boundary conditions for the governing equations are

$$\psi(x,0) = 0, \quad \left.\frac{\partial T}{\partial y}\right|_{x,0} = 0, \quad \psi(x,1) = 0, \quad \left.\frac{\partial T}{\partial y}\right|_{x,1} = 0 \tag{14}$$

$$\psi(0,y) = 0, \quad T(0,y) = 1, \quad \psi(1,y) = 0, \quad T(1,y) = 0 \tag{15}$$

There is no physical boundary condition for the value of the vorticity on a solid boundary. However, an expression can be derived from the stream function equation as $\omega_{\text{wall}} = -\partial^2\psi/\partial\eta^2$, where η is the outward direction normal to the surface.

The local variation in the Nusselt number of the nanofluid can be expressed as

$$\text{Nu} = -\frac{k_{\text{eff}}}{k_f}\left.\frac{\partial T}{\partial\eta}\right|_{\eta=0} \tag{16}$$

3 Results and Discussion

The PDQ method [42–45], with the following nonuniform Chebyshev–Gauss–Lobatto grid point distribution, was used to transform the governing equations into a set of algebraic equations

$$x_i = \frac{1}{2}\left[1 - \cos\left(\frac{i}{n_x}\pi\right)\right], \quad i = 0,1,2,\ldots,n_x$$
$$y_j = \frac{1}{2}\left[1 - \cos\left(\frac{j}{n_y}\pi\right)\right], \quad j = 0,1,2,\ldots,n_y \tag{17}$$

The points in this grid system are more closely spaced in regions near the walls where the large velocity and temperature gradients are expected to develop. The computational results were obtained by the successive over-relaxation (SOR) iteration method for an inclination angle ranging from 0 deg to 90 deg, a Rayleigh number varying from 10^4 to 10^6, two different ratios of the nanolayer thickness to the original particle radius (0.02 and 0.1), and a solid volume fraction ranging from 0% to 20%. Five types of nanoparticles (Cu, Ag, CuO, Al_2O_3, and TiO_2) were considered. Water

Table 1 Thermophysical properties of base fluid and nanoparticles

Property	Water	Cu	Ag	CuO	Al_2O_3	TiO_2
ρ (kg/m^3)	997.1	8933	10500	6500	3970	4250
C_p (J/kg K)	4179	385	235	536	765	686
k (W/m K)	0.613	400	429	20	40	9
$\alpha \times 10^7$ (m^2/s)	1.47	1163.1	1738.6	57.5	131.7	30.7
$\beta_T \times 10^6$ (1/K)	210	51	54	51	24	24

(Pr=6.2) served as the base fluid. The thermophysical properties of the fluid and solid phases are shown in Table 1. The convergence criteria were chosen as $|R|_{\max} \leq 10^{-5}$, where $|R|_{\max}$ is the maximum absolute residual value for the vorticity, stream function, and temperature equations.

A series of grid systems of up to 31×31 points was used to obtain a grid-independent mesh size. The results show that when the mesh size is above 26×26, Nu_a along the hot wall and $|\psi|_{\max}$ remain the same (see Table 2). Therefore, 31×31 was used as the mesh size in this study.

In order to validate the numerical code, a solution for the enclosure filled with air (Pr=0.71) was also obtained and compared with the benchmark results obtained by De Vahl Davis [46] through a standard finite-difference method. The results presented in Table 3 show that there is an excellent agreement between the results of the PDQ method and the benchmark results of Ref. [46]. The numerical code was also validated for several other cases that were different from the aforementioned case (see Refs. [27–30]).

The flow and energy transport in the enclosure for the copper nanofluid case are shown in Figs. 2 and 3 for various values of the inclination angle, ratios of the nanolayer thickness to the original particle radius, solid volume fractions, and the Rayleigh numbers. The heated fluid rises along the left wall as a result of buoyancy forces until it reaches near the top wall, where it turns rightward, toward the sidewalls, while it is cooled. Then it turns downward near those walls. Finally, the restriction imposed by the bottom wall forces the fluid to turn leftward, receiving heat, when it reaches the left wall. The flow path is completed as the colder fluid is entrained to the ascending flow along the heated wall. It can be observed that the flow in the enclosure is unicellular for small values of the Rayleigh number. As the Rayleigh number increases, unicellular flow in the core region breaks up into sev-

Table 2 Grid dependency for a copper-based nanofluid (Ra=10^6)

θ	β	ϕ	Grid size	16×16	21×21	26×26	31×31
0	0.02	0.05	Nu_a	9.80	10.02	9.97	9.96
			$\lvert\psi\rvert_{\max}$	22.37	22.28	22.38	22.39
		0.20	Nu_a	11.97	11.97	11.93	11.92
			$\lvert\psi\rvert_{\max}$	31.40	31.72	31.64	31.65
	0.1	0.05	Nu_a	10.08	10.30	10.25	10.24
			$\lvert\psi\rvert_{\max}$	23.01	22.94	23.01	23.02
		0.20	Nu_a	13.24	13.21	13.17	13.16
			$\lvert\psi\rvert_{\max}$	34.74	34.83	34.86	34.77
45	0.02	0.05	Nu_a	9.61	9.79	9.76	9.76
			$\lvert\psi\rvert_{\max}$	45.37	44.76	44.83	44.86
		0.20	Nu_a	11.73	11.65	11.63	11.63
			$\lvert\psi\rvert_{\max}$	59.20	59.02	59.16	59.18
	0.1	0.05	Nu_a	9.89	10.07	10.03	10.03
			$\lvert\psi\rvert_{\max}$	46.48	45.87	45.89	45.95
		0.20	Nu_a	12.96	12.85	12.83	12.83
			$\lvert\psi\rvert_{\max}$	64.97	64.62	64.51	64.49
90	0.02	0.05	Nu_a	5.45	4.56	4.65	4.63
			$\lvert\psi\rvert_{\max}$	50.48	35.55	35.07	34.98
		0.20	Nu_a	9.42	9.50	9.49	9.49
			$\lvert\psi\rvert_{\max}$	97.12	98.95	98.72	98.78
	0.1	0.05	Nu_a	5.32	4.71	4.80	4.78
			$\lvert\psi\rvert_{\max}$	47.32	36.41	36.08	35.98
		0.20	Nu_a	10.55	10.58	10.58	10.58
			$\lvert\psi\rvert_{\max}$	105.56	107.54	107.44	107.48

Table 3 Validation of the numerical code

	Ra=10^4		Ra=10^5		Ra=10^6	
	De Vahl Davis [46]	Present	De Vahl Davis [46]	Present	De Vahl Davis [46]	Present
$\lvert\psi\rvert_{\max}$	-	5.07	9.61	9.60	16.75	16.72
Nu_a	2.24	2.24	4.52	4.52	8.80	8.82
$\mathrm{Nu}_{\max}$	3.53	3.53	7.72	7.70	17.93	17.56
$\mathrm{Nu}_{\min}$	0.59	0.59	0.73	0.73	0.99	0.98

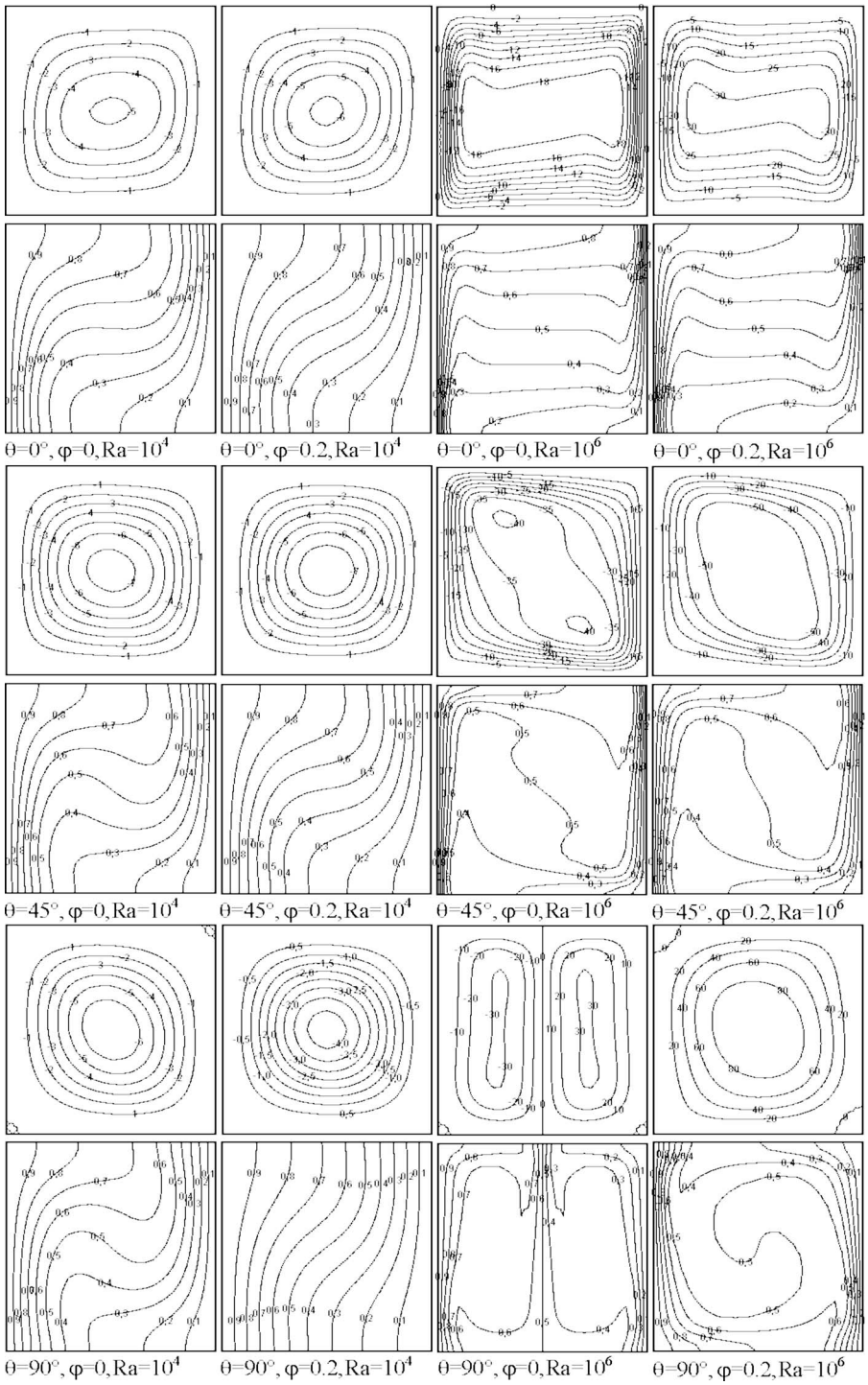

Fig. 2 Streamlines and isotherms of a copper-based nanofluid for β=0.02

eral cells. As may be observed from the figures, the flow structure evolutes toward the boundary layer regime with increasing Rayleigh numbers. The development of the boundary layer regime with increasing Rayleigh numbers is clearly illustrated by the increasing steepness of the velocity and temperature profiles near the walls, as well as by the formation of a plateau in the core region of the flow. The figures reveal that for a particular Rayleigh number, the strength of circulation increases with an increasing solid volume fraction. This is due to the increase in vertical velocity with increasing thermal energy transport from the hot wall to the fluid particles. This case will also cause a decrease in the critical Rayleigh number. This is consistent with the results of Ref. [47]. He found that the presence of nanoparticles decreases the critical Rayleigh number and therefore enhances heat transfer. As can also be seen from the figure, the multicellular flow in the core region disappears with an increasing solid volume fraction, due to the increase in vertical velocity; as a result, the deformation in the isotherms in the core region decreases. Note that an increase in the viscous forces with increasing solid volume fraction is also a fact, although it does not compensate for the increase in the thermal energy from the hot wall to the nanofluid due to increased thermal conductivity. Hence, convective circulation strengthens

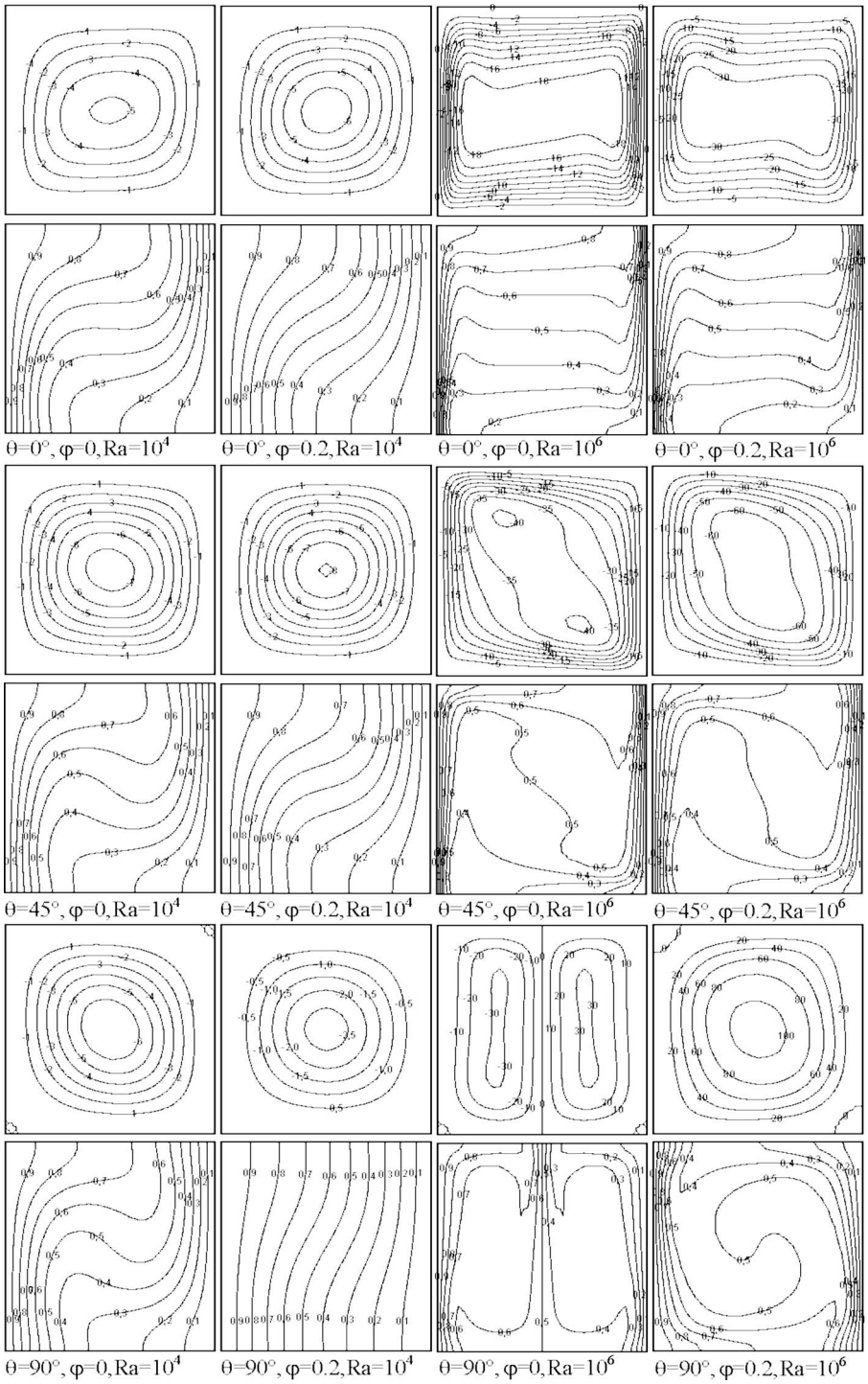

Fig. 3 Streamlines and isotherms of a copper-based nanofluid for β=0.1

with increasing solid volume fraction. Note also that with an increasing solid volume fraction, the isotherms become gradually parallel to the isothermal walls for low values of the Rayleigh number. As the volume fraction increases, thermal diffusion takes on higher values. Therefore, the isotherms become gradually parallel to the isothermal walls. As may be observed from the figures, thermal stratification in the core region is reduced with an increasing inclination angle, resulting in a stronger flow field. In the case of θ=90 deg (corresponding to the enclosure heated from below), the flow and heat transfer fields show a special character. It has been demonstrated in the past [48] that multiple steady-state solutions can be obtained for this configuration. Possible solutions are given below. The first solution is the single-cellular and counterclockwise rotating flow [40]. The image of this flow through a vertical mirror, which is rotating clockwise, is also a possible solution. Both solutions yield the same average heat transfer. This kind of solution will be referred to as a S1-type solution. The second kind of solution is a bicellular ascending flow [40]. Its determination requires an adequate initial perturbation of the ψ field. The image of this flow through a horizontal mirror is also a possible solution, characterized by a bicellular descending flow. This kind of solution will be stated as a solution of the S2-type.

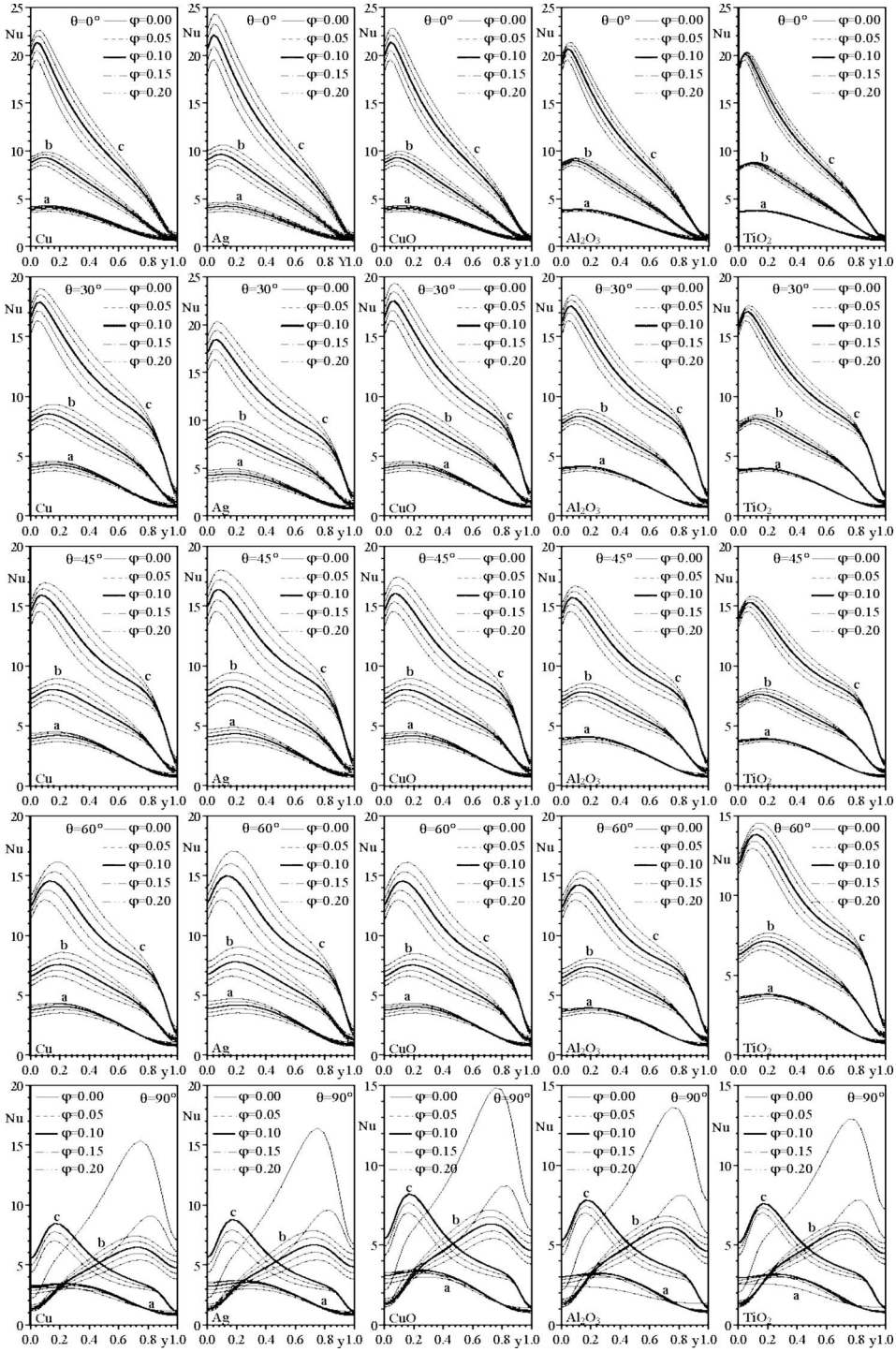

Fig. 4 Local Nusselt number for β=0.02 and (*a*) Ra=10^4, (*b*) Ra=10^5, and (*c*) Ra=10^6

The third kind of solution is bicellular, characterized by the presence of two horizontal cells: one (the negative cell) of which is above the other (the positive cell) [40]. Each cell is in contact with only one active wall, and the heat transfer occurs from the hot wall to the lower cell, from the lower cell to the upper cell (through the interface between the two cells), and finally from the upper cell to the cold surface. In this case, the image from a vertical mirror is also a solution to the problem, leading to the same average heat transfer. This kind of solution will be called a solution of type S3. Obtaining this solution is a special occurrence. In fact, when Ra exceeds the critical Rayleigh number Ra_c, characterizing the transition from steady-state solution of the S1-type toward an oscillatory one, the flow becomes unsteady and bicellular (S3-type) even if the initial conditions are those of a single-cellular flow [40]. As may be observed from Figs. 2 and 3, the numerical code produces an S1-type solution for Ra=10^4, and an S2-type solution for Ra=10^6. The S2-type solution changes to an S1-type for Ra=10^6 with increasing solid volume fraction. The effect of β on the flow and temperature field can be deduced by comparing Figs. 2 and 3. As the nanoparticle radius does not have an important effect on the solid-like nanolayer [49], higher values

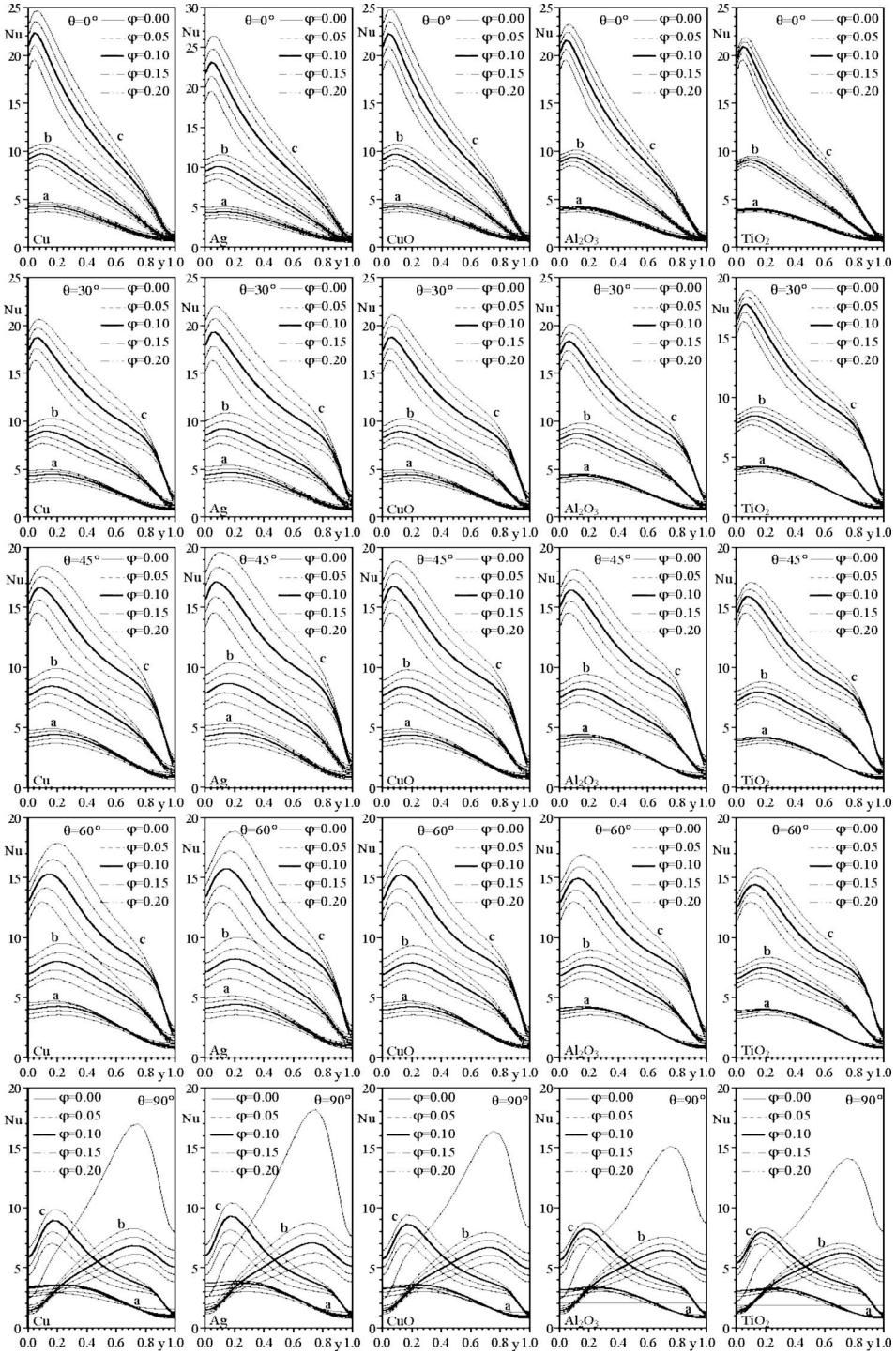

Fig. 5 Local Nusselt number for β=0.1 and (*a*) Ra=10^4, (*b*) Ra=10^5, and (*c*) Ra=10^6

of β correspond to a lower particle radius. As can be observed from the figures, the circulation intensity takes on higher values as the particle radius decreases.

The variation in the local Nusselt number along the hot wall is presented in Figs. 4(*a*)–4(*c*) for β=0.02. As the Rayleigh number increases, the circulation strength increases as a result of higher buoyancy forces. This results in an increase in the local Nusselt number. As a result of a stronger circulation resulting from a higher thermal energy transport from the hot wall to the fluid near the surface, therefore the local Nusselt number takes on higher values with an increasing solid volume fraction. In fact, higher values of thermal conductivity are accompanied by higher values of thermal diffusivity. The high value of thermal diffusivity therefore causes a decrease at the temperature gradient and accordingly increases the thermal boundary thickness. This increase in thermal boundary layer thickness has a negative effect on the Nusselt number; however, according to Eq. (16), the Nusselt number is a multiplication of temperature gradient and the ratio of nanofluid conductivity to the base fluid conductivity. Since the effect of the temperature gradient due to the presence of nanoparticles is much smaller than the thermal conductivity ratio, an enhancement in the Nusselt number is seen with an increase in the volume fraction of

Table 4 Average Nusselt number for inclination angle $\theta=0$ deg

Material		Cu			Ag			CuO			Al_2O_3			TiO_2		
β	φ/Ra	10^4	10^5	10^6	10^4	10^5	10^6	10^4	10^5	10^6	10^4	10^5	10^6	10^4	10^5	10^6
0.02	0.00	2.274	4.722	9.230	2.274	4.722	9.230	2.274	4.722	9.230	2.274	4.722	9.230	2.274	4.722	9.230
	0.05	2.421	5.066	9.962	2.463	5.146	10.106	2.410	5.041	9.908	2.370	4.970	9.783	2.338	4.899	9.639
	0.10	2.553	5.384	10.656	2.643	5.554	10.966	2.535	5.344	10.566	2.449	5.191	10.297	2.386	5.050	10.007
	0.15	2.670	5.674	11.310	2.813	5.946	11.808	2.650	5.631	11.204	2.515	5.385	10.771	2.420	5.173	10.332
	0.20	2.776	5.937	11.921	2.974	6.323	12.633	2.756	5.902	11.822	2.574	5.553	11.206	2.445	5.270	10.612
0.1	0.05	2.483	5.202	10.237	2.526	5.284	10.386	2.466	5.165	10.160	2.428	5.098	10.043	2.387	5.008	9.860
	0.10	2.679	5.662	11.227	2.774	5.841	11.554	2.651	5.599	11.089	2.566	5.449	10.830	2.484	5.267	10.454
	0.15	2.866	6.105	12.201	3.020	6.398	12.739	2.829	6.027	12.022	2.692	5.780	11.594	2.567	5.500	11.011
	0.20	3.052	6.537	13.163	3.267	6.962	13.953	3.005	6.452	12.966	2.824	6.095	12.342	2.646	5.711	11.534

nanoparticles. The similar dependency of the Nusselt number to the nanoparticle concentration was also obtained by Heris and co-workers [49,50] who made an experimental investigation on convective heat transfer of oxide nanofluids. As may be observed from the figures, the local Nusselt numbers for all nanofluids taken into consideration in this study have similar forms; only their magnitudes take on different values. The local Nusselt number for nanoparticles with a higher thermal conductivity (such as Ag and Cu) has higher values. This is because of the fact that thermal energy transport from the hot wall is higher for nanoparticles with higher thermal conductivities. This results in an increase in convection intensity and therefore the temperature gradient on the surface and local Nusselt number takes higher values. As shown in the figures, isotherms in the core region for a vertical enclosure are nearly horizontal, while they are oblique for an inclined enclosure. Therefore, for a vertical enclosure, the temperature of the fluid directed from the cold surface to the base of the hot surface is colder, while the temperature of the fluid in the lower part of the hot surface is higher than the corresponding fluid temperature in an inclined enclosure. As a result, the local Nusselt number for a vertical enclosure shows larger changes along the hot wall compared with the corresponding local Nusselt number for an inclined enclosure. For the inclination angle $\theta=90$ deg, the values of local Nusselt numbers are lower than that of other values of inclination angles due to the reduced value of velocity. For high values of the Rayleigh number, the Rayleigh–Bénard type flow is formed inside the enclosure for low values of nanoparticle volume fraction. Therefore, two maximum points for the local Nusselt number are formed. As the nanoparticle volume fraction increases, the Rayleigh–Bénard type flow begins to break down and a relatively stronger clockwise circulation takes place in the flow field; therefore, the local Nusselt number takes relatively higher values. The variation in the local Nusselt number for a smaller value of the nanoparticle radius $\beta=0.01$ is presented in Figs. 5(*a*)–5(*c*). It can be observed that the local heat transfer rate shows a considerable enhancement with a decreasing nanoparticle radius. This enhancement in heat transfer can be attributed primarily to the increased volume fraction of the nanolayer per $\phi_{\text{eff}} = \phi\ (1+\beta^3)$ (see Ref. [8] for details). The similar dependency of the heat transfer rate to the nanoparticle radius was also observed by Mirmasoumi and Behzadmehr [51], who studied the effect of the nanoparticle diameter on mixed convection heat transfer in a

Table 5 Average Nusselt number for inclination angle $\theta=30$ deg

Material		Cu			Ag			CuO			Al_2O_3			TiO_2		
β	φ/Ra	10^4	10^5	10^6	10^4	10^5	10^6	10^4	10^5	10^6	10^4	10^5	10^6	10^4	10^5	10^6
0.02	0.00	2.529	5.057	9.609	2.529	5.057	9.609	2.529	5.057	9.609	2.529	5.057	9.609	2.529	5.057	9.609
	0.05	2.695	5.421	10.338	2.742	5.500	10.474	2.683	5.402	10.305	2.639	5.337	10.201	2.603	5.260	10.049
	0.10	2.837	5.763	11.021	2.940	5.930	11.317	2.819	5.737	10.984	2.720	5.597	10.756	2.651	5.441	10.450
	0.15	2.950	6.088	11.656	3.119	6.354	12.138	2.935	6.063	11.646	2.767	5.837	11.275	2.669	5.602	10.811
	0.20	3.029	6.401	12.241	3.274	6.778	12.941	3.025	6.383	12.291	2.784	6.059	11.760	2.658	5.741	11.131
0.1	0.05	2.764	5.567	10.620	2.812	5.647	10.761	2.746	5.536	10.566	2.703	5.476	10.471	2.658	5.377	10.278
	0.10	2.975	6.063	11.600	3.084	6.238	11.911	2.946	6.013	11.522	2.845	5.879	11.308	2.757	5.678	10.913
	0.15	3.155	6.557	12.545	3.339	6.842	13.066	3.124	6.495	12.481	2.950	6.274	12.126	2.821	5.963	11.516
	0.20	3.303	7.061	13.467	3.575	7.475	14.241	3.277	6.989	13.452	3.025	6.663	12.931	2.854	6.232	12.086

Table 6 Average Nusselt number for inclination angle $\theta=45$ deg

Material		Cu			Ag			CuO			Al_2O_3			TiO_2		
β	φ/Ra	10^4	10^5	10^6	10^4	10^5	10^6	10^4	10^5	10^6	10^4	10^5	10^6	10^4	10^5	10^6
0.02	0.00	2.545	4.915	9.070	2.545	4.915	9.070	2.545	4.915	9.070	2.545	4.915	9.070	2.545	4.915	9.070
	0.05	2.717	5.285	9.758	2.763	5.356	9.882	2.705	5.268	9.733	2.662	5.214	9.645	2.626	5.136	9.500
	0.10	2.864	5.642	10.413	2.967	5.793	10.684	2.846	5.616	10.384	2.746	5.496	10.190	2.677	5.340	9.898
	0.15	2.976	5.988	11.035	3.148	6.232	11.480	2.962	5.960	11.025	2.789	5.762	10.709	2.692	5.525	10.264
	0.20	3.044	6.328	11.632	3.299	6.677	12.275	3.046	6.302	11.660	2.788	6.012	11.203	2.666	5.690	10.599
0.1	0.05	2.787	5.430	10.026	2.835	5.502	10.153	2.769	5.401	9.980	2.728	5.352	9.901	2.682	5.253	9.718
	0.10	3.003	5.942	10.964	3.113	6.101	11.250	2.974	5.893	10.895	2.872	5.779	10.716	2.784	5.577	10.339
	0.15	3.179	6.461	11.893	3.369	6.723	12.373	3.151	6.395	11.822	2.968	6.202	11.523	2.842	5.888	10.936
	0.20	3.308	6.996	12.832	3.595	7.383	13.542	3.292	6.913	12.775	3.017	6.624	12.334	2.855	6.186	11.516

Table 7 Average Nusselt number for inclination angle θ=60 deg

Material		Cu			Ag			CuO			Al_2O_3			TiO_2		
β	φ/Ra	10^4	10^5	10^6	10^4	10^5	10^6	10^4	10^5	10^6	10^4	10^5	10^6	10^4	10^5	10^6
0.02	0.00	2.496	4.687	8.396	2.496	4.687	8.396	2.496	4.687	8.396	2.496	4.687	8.396	2.496	4.687	8.396
	0.05	2.670	5.062	9.086	2.714	5.127	9.201	2.658	5.042	9.046	2.616	4.994	8.962	2.580	4.918	8.826
	0.10	2.815	5.428	9.762	2.916	5.568	10.014	2.798	5.395	9.694	2.699	5.286	9.509	2.631	5.133	9.231
	0.15	2.919	5.785	10.421	3.092	6.014	10.829	2.908	5.745	10.341	2.730	5.565	10.041	2.638	5.332	9.614
	0.20	2.966	6.137	11.076	3.231	6.466	11.654	2.977	6.094	10.991	2.703	5.830	10.564	2.592	5.513	9.979
0.1	0.05	2.739	5.204	9.343	2.785	5.270	9.461	2.721	5.173	9.282	2.681	5.128	9.206	2.636	5.033	9.033
	0.10	2.951	5.723	10.298	3.060	5.871	10.564	2.923	5.666	10.186	2.822	5.564	10.014	2.735	5.366	9.654
	0.15	3.113	6.252	11.269	3.306	6.499	11.708	3.090	6.172	11.117	2.898	5.999	10.831	2.780	5.689	10.265
	0.20	3.209	6.799	12.289	3.509	7.164	12.921	3.207	6.697	12.092	2.910	6.434	11.677	2.764	6.002	10.878

horizontal tube, and by Anoop et al. [52], who performed an experimental investigation on the convective heat transfer in the developing region of tube flow.

The variation in the average Nusselt number with the Rayleigh number is shown in Tables 4–8 for various values of the governing parameters. The average heat transfer rate takes on different values, ordered from the highest to lowest, in Ag, Cu, CuO, Al_2O_3, and TiO_2. As can be inferred from the results in Tables 4–8, the average Nusselt number does not change significantly with the increasing solid volume fraction for low values of the Rayleigh number, as a result of weak convection. On the other hand, for high values of the Rayleigh number, there is a remarkable increase in heat transfer with increasing solid volume fractions. It can also be concluded from the results that the average Nusselt number shows nearly a linear variation with the volume fraction. The effect of the inclination angle on the average Nusselt number can be revealed by comparing the results in Tables 4–8. The average heat transfer rate shows an increasing trend with an increasing inclination angle and a peak value is detected. Beyond the peak point, the foregoing trend reverses such that the heat transfer rate decreases with further increases in the inclination angle. The minimum heat transfer rates take place for θ=90 deg due to the low velocity encountered at this angle. The maximum heat transfer takes place at θ=45 deg for Ra=10^4 and at θ=30 deg for Ra=10^5 and 10^6.

The percentage increase in the average heat transfer rate is shown in Table 9, which occurs when the solid volume fraction is increased from ϕ=0 to ϕ=0.2. The thickness of the liquid layering is about 1–2 nm at most [53,54]. Therefore, the nanoparticle radius used in practice corresponds to β=0.02 or β=0.1. As can be seen from the table, in this case, an increase in the average heat transfer rate, up to 44% for Ra=10^4, 53% for Ra=10^5, and 54% for Ra=10^6, occurs if the special case of θ=90 deg, which also produces the minimum heat transfer rates, is not taken into consideration. As for θ=90 deg, the heat transfer enhancement reaches 21% for Ra=10^4, up to 44% for Ra=10^5, and up to 138% for Ra=10^6. At Ra=10^4, for Al_2O_3-based and TiO_2-based nanofluids, which have a relatively small thermal conductivity, an unexpected decrease is observed in the heat transfer rate with in-

Table 8 Average Nusselt number for inclination angle θ=90 deg

Material		Cu			Ag			CuO			Al_2O_3			TiO_2		
β	φ/Ra	10^4	10^5	10^6	10^4	10^5	10^6	10^4	10^5	10^6	10^4	10^5	10^6	10^4	10^5	10^6
0.02	0.00	2.188	3.877	4.181	2.187	3.877	4.181	2.187	3.877	4.181	2.187	3.877	4.181	2.187	3.877	4.181
	0.05	2.335	4.253	4.632	2.377	4.307	4.693	2.326	4.219	4.582	2.286	4.175	4.530	2.255	4.110	4.458
	0.10	2.431	4.618	5.072	2.534	4.737	5.205	2.424	4.557	4.977	2.313	4.463	4.864	2.264	4.329	4.716
	0.15	2.433	4.974	5.490	2.636	5.165	5.709	2.456	4.892	5.363	2.214	4.742	5.179	2.170	4.5360	4.952
	0.20	2.266	5.320	9.494	2.638	5.596	9.950	2.374	5.227	9.276	1.891	5.013	8.819	1.905	4.729	8.308
0.1	0.05	2.394	4.379	4.775	2.437	4.435	4.838	2.379	4.334	4.712	2.339	4.295	4.664	2.302	4.211	4.571
	0.10	2.533	4.884	5.374	2.647	5.010	5.516	2.521	4.799	5.250	2.399	4.711	5.141	2.339	4.536	4.948
	0.15	2.535	5.397	5.966	2.777	5.605	6.207	2.566	5.276	5.794	2.277	5.131	5.609	2.236	4.856	5.307
	0.20	2.267	5.922	10.574	2.743	6.230	11.086	2.432	5.771	10.277	2.023	5.558	9.827	1.837	5.170	9.125

Table 9 Percentage increase in the average Nusselt number

Material		Cu			Ag			CuO			Al_2O_3			TiO_2		
θ (deg)	β	10^4	10^5	10^6	10^4	10^5	10^6	10^4	10^5	10^6	10^4	10^5	10^6	10^4	10^5	10^6
0	0.02	22	25	29	31	34	37	21	25	28	13	18	21	8	12	15
	0.1	34	38	42	44	47	51	32	37	41	24	29	34	16	21	25
30	0.02	20	27	27	30	34	35	20	26	28	10	20	22	5	14	16
	0.1	31	40	40	41	48	48	30	38	40	20	32	35	13	23	26
45	0.02	20	29	28	30	36	35	20	28	29	10	22	24	5	16	17
	0.1	30	42	42	41	50	49	29	41	41	19	35	36	12	26	27
60	0.02	19	31	32	30	38	39	19	30	31	8	24	26	4	18	19
	0.1	29	45	46	41	53	54	29	43	44	17	37	39	11	28	30
90	0.02	4	37	127	21	44	138	9	35	122	−14	29	111	−13	22	99
	0.1	4	53	153	25	61	165	11	49	146	−7	43	135	−16	33	118

Table 10 A comparison for the average Nusselt number

	ϕ	0	0.04	0.08	0.12	0.16	0.20
Present	$Gr=10^3$	1.94	2.07	2.21	2.34	2.48	2.63
Khanafer et al. [19]	$Gr=10^3$	1.96	2.11	2.25	2.36	2.57	2.75
Present	$Gr=10^4$	4.08	4.41	4.72	5.03	5.33	5.62
Khanafer et al. [19]	$Gr=10^4$	4.07	4.36	4.68	5.00	5.32	5.68

creasing solid volume fraction for an inclination angle of $\theta=90$ deg. With increasing solid volume fractions, the isotherms gradually become parallel to the isothermal walls (see Figs. 2 and 3), which is the conduction solution ($Ra=10^4$), as a result of a weakening clockwise circulation; therefore, the heat transfer rate decreases.

The problem considered in this paper was also studied by Khanafer et al. [19] for the vertical enclosure case. A comparison of the values of the average Nusselt number obtained in the work done by Khanafer et al. [19] and in this work show that there is a reasonably good agreement (see Table 10). Differences between the results can be attributed to the fact that Khanafer et al. [19] used a different model, which was based on the thermal dispersion of nanoparticles, for his thermal conductivity predictions.

4 Conclusion

Heat transfer enhancement of water-based nanofluids in a differentially heated, tilted enclosure is studied numerically for a range of inclination angles, nanoparticle radii, solid volume fractions, and Rayleigh numbers. It may be concluded from the results that suspended nanoparticles substantially increase the heat transfer rate. It may also be concluded that the variation in the average Nusselt number is nearly linear with the solid volume fraction. The results also show that the average heat transfer rate increases with an increasing inclination angle, and a peak value is detected. Beyond the peak point, the foregoing trend reverses and the average heat transfer rate decreases with a further increase in the inclination angle. Minimum heat transfer takes place at $\theta=90$ deg. Maximum heat transfer takes place at $\theta=45$ deg for $Ra=10^4$ and at $\theta=30$ deg for $Ra=10^5$ and 10^6.

Nomenclature

c_p = specific heat at constant pressure
g = gravitational acceleration
Gr = Grashof number
H = height of the enclosure
k = thermal conductivity
L = width of the enclosure
Nu = Nusselt number
n = shape factor
p = pressure
Pr = Prandtl number
R = residue
Ra = Rayleigh number
T = temperature
u = velocity component in the x direction
v = velocity component in the y direction
x = Cartesian coordinate
y = Cartesian coordinate

Greek Symbols

α = thermal diffusivity
β = ratio of the nanolayer thickness to the original particle radius
β_T = thermal expansion coefficient
γ = kinematic viscosity
η = outward variable normal to the surface
φ = solid volume fraction
μ = dynamic viscosity
θ = inclination angle
ρ = density
Ψ = sphericity
ψ = stream function
ω = vorticity

Subscripts

a = average
C = cold
eff = effective
f = fluid
H = hot
o = reference value
s = solid

Superscript

* = dimensional variable

References

[1] Eastman, J. A., Choi, S. U. S., Yu, W., and Thompson, L. J., 2001, "Anomalously Increased Effective Thermal Conductivity of Ethylene Glycol-Based Nanofluids Containing Copper Nanoparticles," Appl. Phys. Lett., **78**, pp. 718–720.
[2] Choi, S. U. S., Zhang, Z. G., Yu, W., Lockwood, F. E., and Grulke, E. A., 2001, "Anomalous Thermal Conductivity Enhancement in Nanotube Suspension," Appl. Phys. Lett., **79**, pp. 2252–2254.
[3] Xuan, Y., and Li, Q., 2000, "Heat Transfer Enhancement of Nanofluids," Int. J. Heat Fluid Flow, **21**, (1), pp. 58–64.
[4] Das, S. K., Putra, N., Thiesen, P., and Roetzel, W., 2003, "Temperature Dependence of Thermal Conductivity Enhancement for Nanofluids," ASME J. Heat Transfer, **125**, pp. 567–574.
[5] Keblinski, P., Phillpot, S. R., Choi, S. U. S., and Eastman, J. A., 2002, "Mechanisms of Heat Flow in Suspensions of Nano-sized Particles (Nanofluids)," Int. J. Heat Mass Transfer, **45**, pp. 855–863.
[6] Maxwell, J. C., 1881, *A Treatise on Electricity and Magnetism*, Clarendon, Oxford, UK.
[7] Hamilton, R. L., and Crosser, O. K., 1962, "Thermal Conductivity of Heterogeneous Two-Component Systems," Ind. Eng. Chem. Fundam., **1**, pp. 187–191.
[8] Yu, W., and Choi, S. U. S., 2003, "The Role of Interfacial Layers in the Enhanced Thermal Conductivity of Nanofluids: A Renovated Maxwell Model," J. Nanopart. Res., **5**, pp. 167–171.
[9] Brinkman, H. C., 1952, "The Viscosity of Concentrated Suspensions and Solutions," J. Chem. Phys., **20**, pp. 571–581.
[10] Xuan, Y., Li, Q., Xuan, Y., and Li, Q., 1999, "Experimental Research on the Viscosity of Nanofluids," Report of Nanjing University of Science and Technology.
[11] Xuan, Y., and Li, Q., 2003, "Investigation on Convective Heat Transfer and Flow Features of Nanofluids," ASME J. Heat Transfer, **125**, pp. 151–155.
[12] Eastman, J. A., Choi, S. U. S., Li, S., Soyez, G., Thompson, L. J., and DiMelfi, R. J., 1999, "Novel Thermal Properties of Nanostructured Materials," J. Metastable Nanocryst. Mater., **2–6**, pp. 629–634.
[13] Wen, D., and Ding, Y., 2004, "Experimental Investigation Into Convective Heat Transfer of Nanofluids at the Entrance Region Under Laminar Flow Conditions," Int. J. Heat Mass Transfer, **47**, pp. 5181–5188.
[14] Maiga, S. E. B., Nguyen, C. T., Galanis, N., and Roy, G., 2004, "Heat Transfer Behaviours of Nanofluids in a Uniformly Heated Tube," Superlattices Microstruct., **35**, pp. 543–557.
[15] Maiga, S. E. B., Palm, S. J., Nguyen, C. T., Roy, G., and Galanis, N., 2005, "Heat Transfer Enhancement by Using Nanofluids in Forced Convection Flows," Int. J. Heat Fluid Flow, **26**, pp. 530–546.
[16] Akbarinia, A., and Behzadmehr, A., 2007, "Numerical Study of Laminar Mixed Convection of a Nanofluid in Horizontal Curved Tubes," Appl. Therm. Eng., **27**(8–9), pp. 1327–1337.
[17] Mirmasoumi, S., and Behzadmehr, A., 2008, "Numerical Study of Laminar Mixed Convection of a Nanofluid in a Horizontal Tube Using Two-Phase Mixture Model," Appl. Therm. Eng., **28**(7), pp. 717–727.
[18] Izadi, M., Behzadmehr, A., and Jalali-Vahida, D., 2009, "Numerical Study of

Developing Laminar Forced Convection of a Nanofluid in an Annulus," Int. J. Therm. Sci., **48**(11), pp. 2119–2129.
[19] Khanafer, K., Vafai, K., and Lightstone, M., 2003, "Buoyancy Driven Heat Transfer Enhancement in a Two-Dimensional Enclosure Utilizing Nanofluids," Int. J. Heat Mass Transfer, **46**, pp. 3639–3653.
[20] Santra, A. K., Sen, S., and Chakraborty, N., 2008, "Study of Heat Transfer Augmentation in a Differentially Heated Square Cavity Using Copper–Water Nanofluid," Int. J. Therm. Sci., **47**, pp. 1113–1122.
[21] Hwang, K. S., Lee, J. H., and Jang, S. P., 2007, "Buoyancy-Driven Heat Transfer of Water-Based Al_2O_3 Nanofluids in a Rectangular Cavity," Int. J. Heat Mass Transfer, **50**, pp. 4003–4010.
[22] Jou, R.-Y., and Tzeng, S.-C., 2006, "Numerical Research of Nature Convective Hat Transfer Enhancement Filled With Nanofluids in Rectangular Enclosures," Int. Commun. Heat Mass Transf., **33**, pp. 727–736.
[23] Oztop, H. F., and Abu-Nada, E., 2008, "Numerical Study of Natural Convection in Partially Heated Rectangular Enclosures Filled With Nanofluids," Int. J. Heat Fluid Flow, **29**(5), pp. 1326–1336.
[24] Aminossadati, S. M., and Ghasemi, B., 2009, "Natural Convection Cooling of a Localised Heat Source at the Bottom of a Nanofluid-Filled Enclosure," Eur. J. Mech. B/Fluids, **28**(5), pp. 630–640.
[25] Tiwari, R. K., and Das, M. K., 2007, "Heat Transfer Augmentation in a Two-Sided Lid-Driven Differentially Heated Square Cavity Utilizing Nanofluids," Int. J. Heat Mass Transfer, **50**, pp. 2002–2018.
[26] Koo, J., and Kleinstreuer, C., 2005, "Laminar Nanofluid Flow in Microheat-Sinks," Int. J. Heat Mass Transfer, **48**, pp. 2652–2661.
[27] Kahveci, K., 2007, "Numerical Simulation of Natural Convection in a Partitioned Enclosure Using PDQ Method," Int. J. Numer. Methods Heat Fluid Flow, **17**(4), pp. 439–456.
[28] Kahveci, K., 2007, "Natural Convection in a Partitioned Vertical Enclosure Heated With a Uniform Heat Flux," ASME J. Heat Transfer, **129**, pp. 717–726.
[29] Kahveci, K., 2007, "A Differential Quadrature Solution of Natural Convection in an Enclosure With a Finite Thickness Partition," Numer. Heat Transfer, Part A, **51**(10), pp. 979–1002.
[30] Kahveci, K., and Öztuna, S., 2008, "A Differential Quadrature Solution of MHD Natural Convection in an Inclined Enclosure With a Partition," ASME J. Fluids Eng., **130**, p. 021102.
[31] Öztuna, S., 2007, "A Differential Quadrature Solution of Natural Convection in an Enclosure With a Partial Partition," Numer. Heat Transfer, Part A, **52**(11), pp. 1009–1026.
[32] Oztop, H. F., and Dagtekin, I., 2004, "Mixed Convection in Two-Sided Lid-Driven Differentially Heated Square Cavity," Int. J. Heat Mass Transfer, **47**, pp. 1761–1769.
[33] Bilgen, E., and Oztop, H., 2005, "Natural Convection Heat Transfer in Partially Open Inclined Square Cavities," Int. J. Heat Mass Transfer, **48**(8), pp. 1470–1479.
[34] Oztop, H., and Bilgen, E., 2006, "Natural Convection in Differentially Heated and Partially Divided Square Cavities With Internal Heat Generation," Int. J. Heat Fluid Flow, **27**, pp. 466–475.
[35] Oztop, H. F., 2007, "Natural Convection in Tilted Porous Enclosures With Discrete Heat Sources," Journal of Energy, Heat Mass Transfer, **29**, pp. 83–94.
[36] Oztop, H. F., 2007, "Natural Convection in Partially Cooled and Inclined Porous Rectangular Enclosures," Int. J. Therm. Sci., **46**, pp. 149–156.
[37] Lamsaadi, M., Naimi, M., Hasnaoui, M., and Mamou, M., 2006, "Natural Convection in a Vertical Rectangular Cavity With a Non-Newtonian Power Law Fluid and Subjected to a Horizontal Temperature Gradient," Numer. Heat Transfer, Part A, **49**, pp. 969–990.
[38] Bazylak, A., Djilali, N., and Sinton, D., 2006, "Natural Convection in an Enclosure With Distributed Heat Sources," Numer. Heat Transfer, Part A, **49**, pp. 655–667.
[39] Nakhi, A. B., and Chamkha, A. J., 2006, "Effect of Length and Inclination of a Thin Fin on Natural Convection in a Square Enclosure," Numer. Heat Transfer, Part A, **50**(3), pp. 389–407.
[40] Ridouane, E. H., Hasnaoui, M., Amahmid, A., and Raji, A., 2004, "Interaction Between Natural Convection and Radiation in a Square Cavity Heated From Below," Numer. Heat Transfer, Part A, **45**(3), pp. 289–311.
[41] Gill, A. E., 1966, "The Boundary Layer Regime for Convection in a Rectangular Cavity," J. Fluid Mech., **26**, pp. 515–536.
[42] Shu, C., 2000, *Differential Quadrature and Its Application in Engineering*, Springer-Verlag, Berlin.
[43] Bellman, R. E., Kashef, B. G., and Casti, J., 1972, "Differential Quadrature: A Technique for the Rapid Solution of Nonlinear Partial Differential Equations," J. Comput. Phys., **10**, pp. 40–52.
[44] Shu, C., 1992, "Generalized Differential-Integral Quadrature and Application to the Simulation of Incompressible Viscous Flows Including Parallel Computation," Ph.D. thesis, University of Glasgow, Glasgow, UK.
[45] Shu, C., and Richards, B. E., 1992, "Application of Generalized Differential Quadrature to Solve Two-Dimensional Incompressible Navier–Stokes Equations," Int. J. Numer. Methods Fluids, **15**, pp. 791–798.
[46] De Vahl Davis, G. V., 1983, "Natural Convection of Air in a Square Cavity: A Benchmark Numerical Solution," Int. J. Numer. Methods Fluids, **3**, pp. 249–264.
[47] Tzou, D. Y., 2008, "Instability of Nanofluids in Natural Convection," ASME J. Heat Transfer, **130**, p. 072401.
[48] Hasnaoui, M., Bilgen, E., and Vasseur, P., 1992, "Natural Convection Heat Transfer in Rectangular Cavities Partially Heated From Below," J. Thermophys. Heat Transfer, **6**(2), pp. 255–264.
[49] Zeinali Heris, S., Etemad, S. G., and Esfahany, M. N., 2006, "Experimental Investigation of Oxide Nanofluids Laminar Flow Convective Heat Transfer," Int. Commun. Heat Mass Transfer, **33**, pp. 529–535.
[50] Zeinali Heris, S., Esfahany, M. N., and Etemad, S. G., 2007, "Experimental Investigation of Convective Heat Transfer of Al_2O_3/Water Nanofluid in Circular Tube," Int. J. Heat Fluid Flow, **28**, pp. 203–210.
[51] Mirmasoumi, S., and Behzadmehr, A., 2008, "Effect of Nanoparticles Mean Diameter on Mixed Convection Heat Transfer of a Nanofluid in a Horizontal Tube," Int. J. Heat Fluid Flow, **29**, pp. 557–566.
[52] Anoop, K. B., Sundararajan, T., and Das, S. K., 2009, "Effect of Particle Size on the Convective Heat Transfer in Nanofluid in the Developing Region," Int. J. Heat Mass Transfer, **52**, pp. 2189–2195.
[53] Wang, B.-X., Zhou, L.-P., and Peng, X.-F., 2003, "A Fractal Model for Predicting the Effective Thermal Conductivity of Liquid With Suspension of Nanoparticles," Int. J. Heat Mass Transfer, **46**, pp. 2665–2672.
[54] Tillman, P., and Hill, J. M., 2007, "Determination of Nanolayer Thickness for a Nanofluid," Int. Commun. Heat Mass Transf., **34**, pp. 399–407.